Received: 15 July 2020 | Accepted: 25 November 2020

DOI: 10.1002/pamm.202000310

Active Damping of Thin Film Shape Memory Alloy Devices

S. Ahmadi[1,2], **K. Jacob**[1], **F. Wendler**[2,*], **A. Padhy**[2], and **M. Kohl**[1]

[1] Karlsruhe Institute of Technology, Institute of Microstructure Technology, Karlsruhe, Germany
[2] Friedrich-Alexander University of Erlangen-Nürnberg, Institute of Materials Simulation, Fürth, Germany

The thermomechanical coupling in shape memory alloys (SMAs) provides an effective mechanism of vibration damping by a cyclic structural phase transition. Here, we present simulations for an active SMA damper device based on a polycrystalline film materials, in which active damping via the one-way shape memory effect is exploited. We apply an extension of a previously reported superelastic model, that combines transition state kinetics with a phase field approach for the case of shock loading. By this approach, we are able to describe the time-resolved active damping performance of the device in agreement with experimental results.

1 Introduction

The large mechanical hysteresis of shape memory alloys (SMAs) under cyclic loading has been examined since decades for the dissipation of energy due to external (seismic, wind) loads of large structures with comparatively low frequencies [1]. On the other hand, SMA thin films showing fast thermal kinetics and large damping capacity are promising for effective vibration control in portable handheld applications. Recently, we studied pre-strained superelastic (SE) SMA films for damping of miniature applications under both harmonic and step loading with a mesoscale model, including the evolution of mechanical strain, temperature and phase fraction [2, 3]. In these cases, decay in specific damping capacity is observed due to the accumulation of martensite during continuous operation. In superelastic (SE) materials, the plateaus observed in the stress-strain characteristics under quasi-stationary loading are caused by a stress induced transformation from the initial austenite (A) to martensite (M) phase and back, in a nearly fully reversible manner. In SMAs showing the shape memory effect (SME), a remanent strain occurs upon unloading, which has to be reset by controlled heating to the A phase for a cyclic operation. This opens up another active damping mechanism, especially useful under shock loading conditions which is examined in this work for miniature bridge devices with transient finite element simulations.

2 Material Characterization and Experimental test-setup

As-received cold-rolled $Ti_{50.18}Ni_{49.82}$ (at %) film of 30 µm thickness is heat treatment at 450°C for 30 minutes to adjust the phase transformation behavior. The phase transformation temperatures of the material are identified from DSC measurement with the temperature sweep between -100°C and 150°C at a rate of 10 °C/min as shown in Fig. 1b. Upon heating from a starting temperature of -100°C, a single peak occurs at $A_p = 53.3$°C indicating a direct transition from martensite to austenite. Upon cooling, austenite phase transforms to martensite through two-stage transformation. The transformation peaks for R and martensite phases are 47.9°C and -5.09°C, respectively.

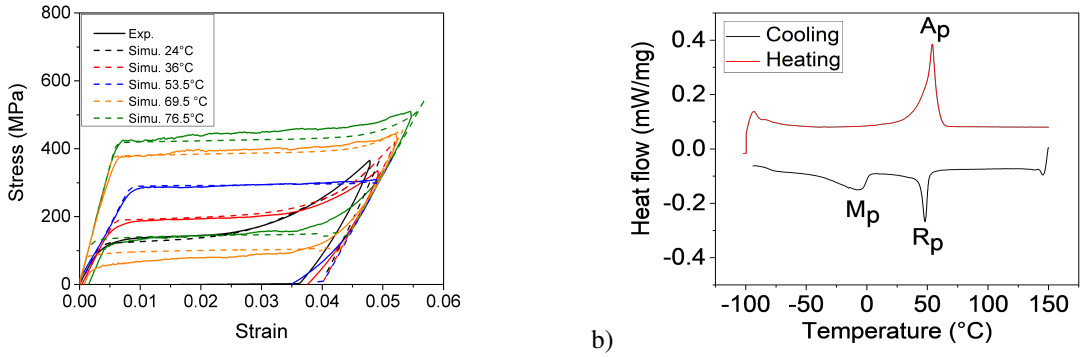

Fig. 1: (a): Experimental and simulated stress-strain loops of the investigated NiTi film during tensile tests at different ambient temperatures as indicated (strain rate $10^{-3}s^{-1}$). (b): DAC measurement showing the transformation peaks of the investigated NiTi film annealed at 450°C.

A test setup has been developed to investigate the free oscillation of a proof mass subjected to pulsed loading. As sketched in Fig. 2a, the test setup consists of a proof mass of 18g attached to eight bridges having a bridge length of 5 mm and width of

* Corresponding author: e-mail frank.wendler@fau.de, phone +49 911 65078-65067, fax +49 911 65078-65066

300 µm. The bridges are pre-strained along in-plane (x-) direction as shown in Fig. 2a. The proof mass is aligned horizontally and excited along (z-) direction using an electromagnet. After introducing the desired loading amplitude, the mass is released by deactivating the electromagnet and the resulting free oscillation of the mass is tracked using a laser displacement sensor. Austenite phase transformation is induced by applying controlled heating pulses across terminals V1 and V2. The current pulse heats up the bridges and mass oscillation is damped by changing the stiffness of the SMA bridges.

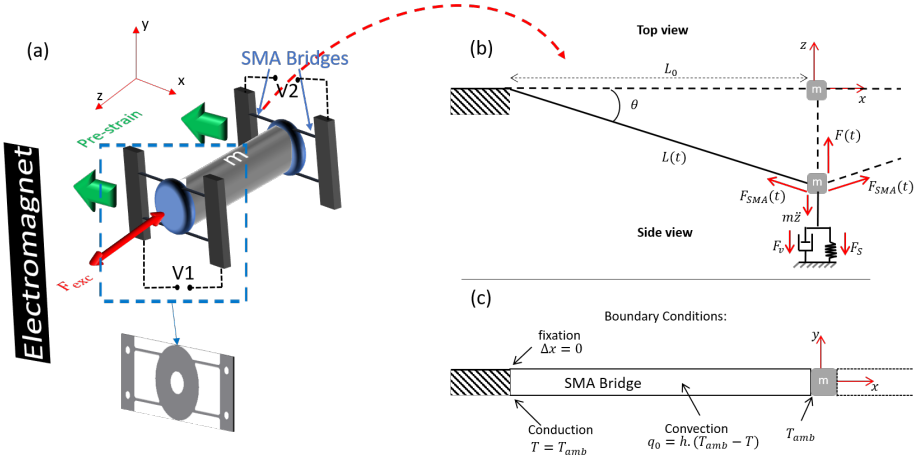

Fig. 2: (a): Schematic of experimental setup of damping device consisting of eight SMA bridges. (b): 2D simulation schematic of one SMA bridge subjected to pre-straining along x-direction and external loading along z-direction. The force balance acting on the proof mass, m, comprises the inertia force, $m\ddot{z}$, time-dependent external force $F(t)$ and the dynamic response of the SMA bridges along tensile direction $F_{SMA}(t)$. (c): Schematic top view of the SMA bridge including mechanical and thermal boundary conditions.

3 Material Model

In the thermomechanical model for the SMA film the momentum balance, the internal energy and the kinetic equations for A and $M_\pm$ phases are solved following the procedure described in [4]. For the film geometry we use a transient elastodynamic equation in tensorial form assuming plane stress conditions, isotropic elasticity with phase-dependent moduli and phase-related eigenstrain. In addition to previous work for a superelastic material in [2], we introduce two different variants M_+ and M_- that represent tensile and compressive adapted deformation. The mixture of both corresponds to twinned martensite which occurs after cooling from A. The kinetic evolution of the state variables $\xi_\alpha(\alpha \in \{A, M_+, M_-\})$ of three phases is treated as a thermal activation process based on rate equations. The corresponding transition probabilities are based on a Gibbs free energy landscape. A/$M_\pm$ interfaces are assumed to carry an interfacial free energy, which is represented by a phase-field term in the kinetic equations, but for M_+/M_- boundaries no interface energy is assumed.

Upon increasing the temperature, a change from one-way to superelastic behavior (closed stress-strain loop) is observed in Fig. 1a at a transition temperature of approximately $T' = 60°$C, associated with a strong increase in Young's modulus. We explain this by the existence of a martensitic rhombohedral (R) phase at lower temperature, as observed in Fig. 1b. In the temperature regime below T' and above M_s =2°C, we explain the quasiplasticity in tensile loading following from the stress induced formation of M_+, rather than detwinning of M_+/M_-, which should happen below $M_f = -28.9°$C. As the transformation strain of R phase is very small (< 0.5 %) compared to M phase, we don't introduce an extra state variable for R. Instead, a temperature dependent modulus is attributed to the A phase, for which we use the sigmoidal transient function

$$E_A(T) = E_R + \frac{1}{2}\left(1 + tanh\left(\frac{T - T'}{\Delta T'}\right)\right)(E_A - E_R). \tag{1}$$

According to Eq. 1, the Young's modulus changes from E_R to E_A within an interval of $\Delta T' = 5°$C. As can be seen from the elastic loading and unloading regions in the stress-strain loops for $T < T'$ in Fig. 1a, the modulus of R phase and martensite agree ($E_R = E_M$).

The pronounced hardening behavior visible in the (quasiplastic) plateau regions for $T < T'$ of Fig. 1a is treated in the model by multiplying the plateau stress σ^{AM} with a function $h(T, \xi_M)$ depending on temperature and martensite fraction, that has been paramatrized with the stress-strain data.

$$\sigma^{AM} = [\sigma_0^{AM} + C^{AM}(T - T_{ref})]h(T, \xi_M) \tag{2}$$

$$\text{with} \quad h(T, \xi_M) = 1 + (116.9 - 0.6657T + 9.55 \cdot 10^{-3}T^2)exp((\xi_M) - 1)/0.15). \tag{3}$$

The simulation model is validated with experimental data and Fig. 1a shows the stress-strain curves at different ambient temperatures during tensile loading at constant strain rate of $10^{-3}s^{-1}$.
The equations for the SMA film are solved for by FEM using COMSOL Multiphysics with solid mechanics, heat transfer and a custom PDE module. Here, mechanical and thermal boundary conditions representing the fixation (left) and the coupling to the moving proof mass are applied, which are depicted in Fig. 2c. As simplification, the ideal case with symmetry conditions for all bridges is assumed, and limited fabrication tolerances of the experimental test setup and possible motion along other directions during free oscillation are not accounted for. The bridges with initial length of L_0 are laterally strained to $L_0(1+\epsilon_{pre})$ at beginning of the simulation as pre-strain condition. As a result, the 1 DOF motion along z-direction of the latter is solved for by the following ODE in COMSOL.

$$m\dot{v} + 8F_{SMA}(t)sin(\theta) + F(t) + c_1\nu + kz = 0, \quad sin(\theta) = \frac{z(t)}{\sqrt{z(t)^2 + L_0^2(1+\epsilon_{pre})^2}} \tag{4}$$

In Eq. 4, $m\dot{v}$ denotes the inertial force of the proof mass, F_{SMA} the in-plane force of the SMA bridge and $F(T)$ the external excitation force. To reduce computational complexity only one SMA film is considered in the FEM simulation and F_{SMA} is multiplied by a factor of eight. Two other terms had to be incorporated and fitted to capture the experimental data: The small elastic force from bending of the SMA bridges at fixation points are included in a spring force with constant $k = 250$ N/m. Even for displacement amplitudes, that are too small to induce martensitic transformation, an exponential decay is observed over long time periods. This is attributed to the effect of air and structural damping, and captured by viscous damping term with factor $c_1 = 0.026$ Ns/m.
In contrast to passive damping devices based on superelastic SMA material, there is no recovery to the initial position after the one-way film material has been deformed. To recover the initial position and deformation always a temperature rise is necessary. In the absence of thermal heating, buckling during motion of the mass towards the center position occurs at low compressive force. Equation 4 is numerically solved after each time step to evaluate the mass position and consequently the mass velocity v. The resulting mass velocity is projected in plane ($v_{BC} = bvsin(\theta)$) and used as the velocity boundary condition on the right side of the bridge where it is connected to the mass. The factor b is defined as a binary function that discovers if the bridge is in buckling state ($b = 0$) by comparing the SMA bridge length from FEM simulation and the distance between fixation and moving mass. By converting the velocity to in-plane, the 3D out-of-plane oscillation of the bridge setup converts to an in-plane tensile loading along the SMA film bridge.

4 Results

Figure 3a shows the time-resolved experimental and simulated mass oscillation for the SMA bridges pre-strained to 1.5% confining mass oscillation within the plateau region, shown in Fig. 1a, under loading conditions. Pre-straining is introduced by ramping up an external force in simulation. The end of pre-straining is indicated by the marking 1 in Fig. 3a. Under this pre-straining condition, the maximum tested out-of-plane loading amplitude in experiment is 1 mm (corresponding to a bridge strain of 3.5%). As shown in Fig. 3a, the bridge device is quasi-statically loaded to an amplitude of 1 mm, and held stationary at this position to stabilize the system as shown between markings 2 and 3 of Fig. 3a. The loading causes self-heating and

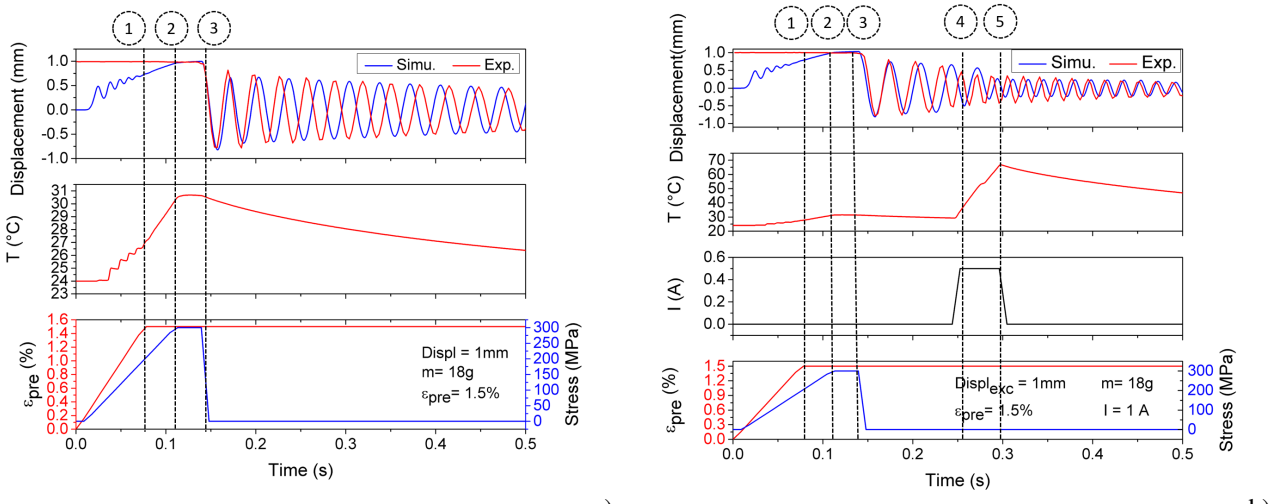

Fig. 3: Time-dependent mass displacement of damper device as well as temperature and pre-strain of SMA bridge for the cases (a) without and (b) with thermal activation. Activation of one-way effect by a current pulse is indicated.

increases the average temperature on the surface of SMA bridge from 7°C to 31°C. Upon releasing, the mass starts to oscillate with a frequency of about 29 Hz. As discussed, the initial phase of SMA at room temperature is assumed to be a mixture of martensite and R phase, whereby the fraction of martensite depends on stress. As no state variable is considered for R phase, it is included in the phase fraction of A phase. In the absence of heating, SMA bridges are in mixed phase state at room temperature and, thus, cannot recover the deformation. In this case, the air drag contributes to the damping of oscillation.

Figure 3 shows simulated and experimental results on load-induced free vibration of a proof mass for the cases without (a) and with thermal activation (b). Thermal activation is achieved by applying a current pulse of 1 A with a duration of 50 ms. The marked numbers of 4 and 5 are indicating the starting and finishing time of heating pulse in Fig. 3b. Due to experimental reasons, the starting time of heating is delayed by 0.24 s. The average temperature over the surface of one SMA bridge rises to 66°C. The thermal pulse leads to a recovery of 15% of austenite fraction. A (the temperature phase) has a higher stiffness in comparison to martensite. Therefore, by increasing the A fraction the oscillation frequency is increasing from 29 Hz to 59 Hz. The deviation between simulated and experimental oscillation frequencies is evaluated less than 3 Hz for both non-heating and heating cases. This deviation we attribute to the complexity of the setup adjustment in experiment and the error of fitting the phenomenological parameters k and c_1. A specific damping capacity of 82% is evaluated for the first oscillation cycle after the heating pulse. In contrast, the simulation for the case without thermal activation results in 36%, for the same oscillation cycle.

5 Conclusions

A model is presented that allows to simulate the mechanical and thermal performance of an active damper device consisting of SMA thin films showing the one-way shape memory effect. As a case study, an experimental setup is established to perform benchmark tests on the load induced free vibration of a proof mass being connected to eight SMA bridges. At maximum excitation displacement and pre-strain within the plateau region, the evolution of load-induced temperature change as well as amplitude and frequency of free oscillation after release is simulated. In particular, the effect of an electrical heat pulse on the change of the oscillation amplitude is well reproduced with an accuracy of 10%. The corresponding maximum damping capacity is determined to be about 82%, while the damping capacity in the absence of active heating is about 36%.

Acknowledgements The authors gratefully acknowledge funding by the German Science Foundation (DFG) within the priority program SPP1897 Calm, Smooth and Smart – Novel Approaches for Influencing Vibrations by Means of Deliberately Introduced Dissipation.
Open access funding enabled and organized by Projekt DEAL.

References

[1] V. Torra, A. Isalgue, F. C. Lovey, M. Sade, J. Therm. Anal. Calorim. **119** 1475–1533 (2015).
[2] S. Ahmadi, K. Jacob, F. Wendler, M. Kohl, Int. J. Smart Nano Mater. **9:3**, 199-215 (2018).
[3] S. Ahmadi, K. Jacob, F. Wendler, M. Kohl, Proc. Appl. Math. Mech. **18:1**, e201800409 (2018).
[4] F. Wendler, H. Ossmer, C. Chluba, E. Quandt, M. Kohl, Acta Mater. **136**, 105-117 (2017).

Appendix

Table 1: Simulation parameters for NiTi.

Parameter	Symbol	NiTi/Value	Parameter	Symbol	NiTi/Value
Critical stress for A-M transformation	σ_{AM}	495 MPa	Elastic modulus of martensite	E_M	32.2×10^9Pa
Critical stress for M-A transformation	σ_{MA}	100 MPa	latent heat	L	22.13 J/kg
Reference temperature	T_{ref}	349.65 K	Thermal conductivity of austenite	$\kappa(A)$	18 W/m/K
Clausius-Clapeyron coefficient (A→M)	C^{AM}	5.8 MPa/K	Thermal conductivity of martensite	$\kappa(M)$	8.6 W/m/K
Clausius-Clapeyron coefficient (M→A)	C^{MA}	6.2 MPa/K	Ambient temperature	$T_{ambient}$	297.15 K
Transformation strain	ϵ_T	0.04	Heat transfer coefficient	h	30 $W/m^2/K$
Elastic modulus of austenite	E_A	70.2×10^9 Pa	Electrical resistivity A	ρ_A	1×10^{-6} Ωm
Elastic modulus of R	E_R	32.2×10^9Pa	Electrical resistivity M	ρ_M	0.8×10^{-6} Ωm

